Reconciling Pyroclastic Flow and Surge: the Multiphase Physics of Pyroclastic Density Currents.

Alain Burgisser, George W. Bergantz

Reconciling Pyroclastic Flow and Surge: the Multiphase Physics of Pyroclastic Density Currents

ALAIN BURGISSER[1]

Alain@gi.alaska.edu, Phone +1 907 474 5606, Fax +1 907 474 7290

Alaska Volcano Observatory, Geophysical Institute, University of Alaska Fairbanks,
Fairbanks, AK 99775-7320 USA

GEORGE W. BERGANTZ

bergantz@u.washington.edu, Phone +1 206 685 4972, Fax +1 206 543 0489

Dept. of Earth and Space Sciences, University of Washington, Box 351310, Seattle,
WA 98195-1310 USA

[1]Corresponding author

Word count: Abstract 231, Main text 5174

1 Table, 7 Figures, 17 Equations, ~13 EPSL Pages

Abstract

Two end-member types of pyroclastic density current are commonly recognized: pyroclastic surges are dilute currents in which particles are carried in turbulent suspension and pyroclastic flows are highly concentrated flows. We provide scaling relations that unify these end-members and derive a segregation mechanism into basal concentrated flow and overriding dilute cloud based on the Stokes number (S_T), the Stability factor (Σ_T) and the Dense-Dilute condition (D_D).

We recognize five types of particle behaviors within a fluid eddy as a function of S_T and Σ_T : *(1)* particles sediment from the eddy, *(2)* particles are preferentially settled out during the downward motion of the eddy, but can be carried during its upward motion, *(3)* particles concentrate on the periphery of the eddy, *(4)* particles settling can be delayed or "fast-tracked" as a function of the eddy spatial distribution, and *(5)* particles remain homogeneously distributed within the eddy. We extend these concepts to a fully turbulent flow by using a prototype of kinetic energy distribution within a full eddy spectrum and demonstrate that the presence of different particle sizes leads to the density stratification of the current. This stratification may favor particle interactions in the basal part of the flow and D_D determines whether the flow is dense or dilute. Using only intrinsic characteristics of the current, our model explains the discontinuous features between pyroclastic flows and surges while conserving the concept of a continuous spectrum of density currents.

1. Introduction

Pyroclastic density currents are rapidly moving mixtures of hot volcanic particles and gas that flow across the ground under the influence of gravity. These multiphase flows consist of particles of various sizes and densities, and a strongly buoyant gas phase. The complex interplay between sedimentation and entrainment, the difficulty of direct observations, and the absence of a direct record of the internal flow structure, makes the study of pyroclastic density currents challenging. The resulting geologic literature is extensive, complex, and sometimes contradictory.

The deposits of pyroclastic density currents vary from stratified to massive. Stratified facies commonly exhibit sedimentary bedforms and the deposit is often weakly controlled by topography, generally mantling the landscape. Massive facies are poorly sorted, often structureless, and pond into depressions. The recognition of these facies has motivated two end-member models of pyroclastic density currents (e.g., [1,2]). Stratified facies are proposed to be the products of a dilute suspension called *pyroclastic surge,* in which particles are carried in turbulent suspension and in a thin bed-load layer. The generally thicker massive facies are the result of highly concentrated *pyroclastic flows* [3].

Mechanical models for both end-members have been developed, based on different assumptions of the physics of the flow. Surge models are assumed to have negligible particle interactions, particle homogenization by turbulence, an exponential sedimentation law, and are often restricted to a single particle size (e.g., [4-6]). Whereas there is little debate that deposition in surge occurs by aggradation, in a layer-by-layer fashion, it is unclear whether pyroclastic flows freeze en masse or gradually sediment

particles. Arguments for en masse deposition include the poorly sorted nature of deposits and the common presence of coarse-tail grading of lithics and/or pumices [7,8]. Sedimentation by freezing implies that the deposit is directly representative of the dynamical state of the moving flow, and this has motivated analogies between pyroclastic flow and hydraulic current or sliding bloc (e.g., [9,10]). Arguments for deposition by aggradation include the existence of compositionally distinct units within some massive deposits and the particle fabric of flow units [11-13]. Considering pyroclastic flows as rapid granular flow is consistent with aggradation [e.g., 14] and some granular models have recently been applied successfully [e.g., 15,16]. However, any unification of the end-members is difficult because the assumptions implicit in each model are incompatible.

Hence, whether pyroclastic flows and surges represent two truly distinct phenomena remains unresolved. The density discontinuities reproduced in experiments of fluidization [17] and high-speed two-phase flow decompression [18], as well as the marked facies diversity of the deposits, are cited in support of a discontinuity between flow and surge. However, deposits composed of a mixture of the two facies, such as the Mt. Pelée 1902 nuée ardente or the Mt. St Helens 1980 blast, motivated a reconsideration of the relationship between the two types [2]. Advocates for a continuous spectrum of density currents proposed that *surges* are density stratified [7,19-21]. They hypothesize that the concentrated base of such a stratified surge can sometimes generate dense underflows that produce the massive deposits characteristic of pyroclastic flows [11,22]. For example, Druitt [21] explains the whole spectrum of facies observed in the 1980 Mt. St Helens lateral blast deposit using the continuum approach. Recently, visual observations

of flow separation at Montserrat [23,24] and Unzen [25] helped to connect processes and related deposits.

Recognizing the paradox inherent in the concept of a continuous spectrum between pyroclastic flows and surges and the basic assumptions commonly used in their modeling, we propose a unifying mechanical model that identifies flows and surges as two entities coexisting in pyroclastic density currents. Our approach accounts for the complexity in the dynamics of multiphase flow introduced by turbulence, and is based on scaling relations of the dominant mechanisms that occur in the currents. Our model focuses on the interplay between particles and turbulence in the absence of particle-particle interaction, and proposes a threshold criterion between dense and dilute conditions, from which the coexistence of surge and flow is derived. We adopt a Lagrangian-Eulerian approach in the dilute regime, however a complete development of a mechanical model of dense granular flow is beyond the scope of this paper.

The idea of linking flows and surges has already been proposed in the literature. While most authors present conceptual models based on geological evidence (e.g., [21,25-29]), few have addressed the fluid mechanics aspect of the problem (e.g., [20,30,31]). Mechanical models of surges assume that turbulence homogenizes the vertical distribution of pyroclasts [5,32,33]. The sedimentation of each class size of particle within the flow/surge is described by the ratio of the particle terminal fall velocity, U_T, and some Eulerian time scale of the flow. The time scale could be given by the horizontal speed of a given volume within the surge [20,33], or by the flow thickness if no velocity gradient within the flow is assumed [5,32]. Coarse particles are calculated to sediment

faster than finer ones, and their increased concentration at the base of the surge generates dense underflows [20].

Our approach relaxes the ad hoc assumption that particles are homogenized and defines dimensionless numbers based on the Lagrangian characteristics of the flow, which allows a refinement of the understanding of particle gathering and dispersal by turbulence. The homogenization of particle distribution is a consequence of the gas phase and the pyroclasts being in dynamic equilibrium when the particles are sufficiently "small". Noting that no quantitative estimate of critical particle size has been given, we question the assumption of homogenization when applied to the whole spectrum of pyroclastic density currents. We expect that the largest clasts can significantly affect the current dynamics and can decouple from the gas phase. By invoking a Lagrangian formulation, we quantify the critical size above which turbulence segregates particles and organizes them within the density current. Turbulence generates unsteady variations of the flow field while gravity sets a steady downward forcing on particles; they cannot be considered as two separate mechanisms that add linearly: their *simultaneous* consideration is necessary [34,35].

Neri and Macedonio [31] recognized the crucial effect of particle size on the dynamics of the flow using a three-phase model of collapsing volcanic columns. They point out that introducing two particle sizes (10 and 200 μm) changes dramatically the behavior of the flow. Motivated by the fact that pyroclastic deposit grain size distributions commonly encompass from −6 to 6 ϕ (6.4 cm to 156 μm), we feel there is a need to assess the role that the whole range of particles size has in the dynamics of the pyroclastic density

currents. The proposed model is based on simple dimensionless numbers and is viewed as a first approach to these complex flows.

2. Segregation model: principles and assumptions

A pyroclastic density current is a fully turbulent parallel shear flow of gas with a significant load of particles with a wide range of sizes and densities. The flow is bounded by the ground at the bottom and by a free surface at the top, and the turbulence generates eddies of various sizes and speeds. In the fully turbulent regime, scalar quantities such as chemical components or temperature are well mixed, but separate phases in the flow such as particles are not necessarily well mixed, forming what has been recognized as 'mesoscale structures' [36]. To understand the interplay between these particles and the turbulence, consider only one given eddy within this spectrum. The acceleration of a sphere in a nonuniform flow is given by the Basset-Boussinesq-Oseen (BBO) equation derived by Maxey and Riley [37], which is the summation of the various forces acting on the particle (see *Appendix*). Following the truncation of the BBO equation by Raju and Meiburg [34], the Lagrangian formulation of a particle motion is, in dimensionless form:

$$\frac{dv}{dt} = \frac{u(t) - v(t)}{S_T} + \frac{e_g}{F_R^2} \tag{1}$$

Where $u(t)$ is the gas velocity, $v(t)$ the particle velocity, e_g the unit vector in gravity direction (see Table 1 for symbol definition). The Stokes number S_T and the particle Froude number F_R are given by:

$$S_T = \frac{t_v}{f} \frac{\Delta U}{\delta} = \frac{1}{f} \frac{\Delta \rho \, d^2}{18\mu} \frac{\Delta U}{\delta} \tag{2}$$

$$F_R = \frac{\Delta U}{\sqrt{g\,\delta}} \qquad\qquad (3)$$

Where $\Delta\rho$ is the density difference between the particle and the gas ($\Delta\rho \approx \rho_p$, with ρ_p being the particle density), d is the particle diameter, μ is the gas dynamic viscosity, ΔU is the eddy rotation speed, δ its diameter, t_v is the response time of particles (Equ. (A2)), f is a drag factor function of the particle Reynolds number Re_p (Equ. (A3)), and g is the acceleration of gravity. Our approach is predicated on the statement that the interaction of particles with this eddy can be understood with two concepts: the Stokes number (S_T) and the Stability factor (Σ_T), which is a ratio of Stokes and Froude numbers.

S_T measures the coupling between gas and particles and is the ratio of the response time of particles t_v (particle reaction to unsteady forcing by gas turbulence), and a time scale of gas motion (eddy rotation time in turbulent flows). S_T controls a self-organization of the particles within an eddy, concentrating or dispersing particle as a function of their density and/or size; small enough particles follow the eddy motion whereas large enough particles are not be affected by the eddy [35]. If $S_T \ll 1$, particles couple with the gas. If $S_T \sim 1$, particles tend to travel at the eddy periphery, possibly escaping from its gyratory motion. Thus, particles with S_T near unity tend to gather at the eddy periphery [38]. If $S_T \gg 1$, particles decouple from turbulence, and particle motion is not governed by the gas phase.

Σ_T assesses the steady gravitational forcing on particles and is a measure of the particle residence within an eddy. We define Σ_T as the ratio of the terminal fall velocity U_T and the eddy rotation velocity ΔU.

$$\Sigma_T = \frac{\rho_p g\, d^2}{18\mu\, f\, \Delta U} = \frac{S_T}{F_R^2} = \frac{U_T}{\Delta U} \tag{4}$$

If $\Sigma_T \gg 1$, particles are influenced by gravity and tend to sediment from the eddy. If $\Sigma_T \ll 1$, particles are influenced by the eddy motion and tend to stay within it (R. Breidenthal, unpub. experimental results). The Stability factor predicts the migration towards the base of the eddy of large and/or dense particles.

2.1 Eddy mechanisms

The simultaneous consideration of S_T and Σ_T with the conditions listed in Table 1 leads to the recognition of five regions within a continuum of particle behaviors (Fig. 1). In the *Fall* zone ($\Sigma_T \gg 1$, $S_T > 1$), particles sediment from the eddy. We define that the lower boundary of the *Fall* zone is reached when ΔU is 30 % superior to U_T (log (Σ_T) = 0.5). In the *Unroll* zone ($\Sigma_T \sim 1$, $S_T > 1$), particles are preferentially settled out where the vertical component of ΔU is maximal downward but can be carried during the upward motion of the eddy. Particle transport becomes asymmetric; the eddy "unrolls" the range of particle sizes lying in this zone. We define that the lower boundary of this asymmetric transport is reached when U_T is 30 % inferior to ΔU (log (Σ_T) = -0.5). In the *Margins* zone ($\Sigma_T < 1$, $S_T \sim 1$), particles concentrate on the periphery of the eddy. Following Hogan and Cuzzi [38], we set the boundary at $S_T = 1$. In the *Turbulent Sedimentation* zone ($\Sigma_T \sim 1$, $S_T < 1$), particle sedimentation is modified by the turbulence structure. Particles settling can be delayed or "fast-tracked" as a function of the eddy spatial distribution [39]. In the *Homogenous Transport* zone ($\Sigma_T \ll 1$, $S_T \ll 1$), particles remain homogeneously carried within the eddy. Since particles in the *Homogenous Transport* zone are dynamically

"attached" to the gas, we can assume that the flow satisfies the criteria for the application of mixture theory. The flow can be considered as a heavy gas, with a total density equal to the gas density plus the particle load of the *Homogenous Transport* zone. We define this condition as "particle homogenization". According to the boundaries defined above, the conditions $S_T = 1$ and $\Sigma_T < 1$ define the critical size above which the homogenization assumption no longer holds. Figure 1 shows the pattern of particle behavior defined by a 10-m wide eddy spinning up to 50 m/s. We choose this relatively small size to account for the reducing effect of the density stratification on eddy sizes (see *2.3 The density profile*). Using the limits between the domains in a quantitative fashion, these conditions would define a median critical size of 0.75 ϕ (0 ϕ at 20 m/s and 1.5 ϕ at 50 m/s). The change of eddy size of an order of magnitude will influence the median critical size by a factor 3.5 (Fig. 2).

2.2 The kinetic energy spectrum

The concepts developed for one eddy can be extended to a fully turbulent flow by using a prototype of the kinetic energy distribution within a full eddy spectrum. Eddies generated by turbulence are represented by a kinetic energy spectrum in Fourier space. The dimension of one eddy can be expressed as a wave number κ and its rotational speed as the kinetic energy per unit mass:

$$E(\kappa)\kappa = \frac{1}{2}\Delta U^2(\kappa) \tag{5}$$

$$\kappa = \frac{4\pi}{\delta} \tag{6}$$

Where $E(\kappa)$ corresponds to the kinetic energy spectrum in Fourier space integrated over a three-dimensional vortex of radius κ and $\Delta U(\kappa)$ is the characteristic speed of this vortex [40]. This spectrum describes how the energy is transferred from the injection frequency κ_i to *(1)* the smaller scale (higher wave numbers) at a rate $\varepsilon \sim \kappa^{-5/3}$ (Kolmogorov's law of decay) and *(2)* to the larger scale at a rate $\sim \kappa^4$ [40]. The largest possible scale is on the order of the flow height for incompressible flows, and the smallest scale we consider is on the order of the particle size. The total kinetic energy is related to $E(\kappa)$ by:

$$\frac{1}{2}U_{rms}{}^2 = \int E(\kappa)\,d\kappa \tag{7}$$

Where U_{rms} is the root-mean-square velocity of the gas. Given a prototype of $E(\kappa)$, the five domains of particle behavior defined above can be transposed from a ΔU-δ space to an E-κ space for any specific particle size (Fig. 3). In a first approach, we use the prototype of energy spectrum for a free decaying three-dimensional isotropic turbulence described by Métais and Lesieur [41], noting that spectrum prototypes for shear flow have a similar form [42]:

$$E(\kappa) = A\kappa^8 e^{-4\left(\frac{\kappa}{\kappa_i}\right)^2} \tag{8}$$

Equation (7) gives $A \cong 44 U_{rms}^2 / \kappa_i^9$ and the space transposition can be done with Equs. (5)-(8). The dynamic behavior of particles of a specific size within a flow can henceforth be characterized for a given kinetic energy spectrum (Fig. 3B).

In the Eddy Mechanism section, we have characterized particle behavior in a single eddy. The extension to a full spectrum of eddies allows us to relate the size of eddies to their speed (Equ. (8) and Fig. 3B), and enables us to understand the behavior of all particle sizes in a full spectrum of turbulence (Fig. 4, with the same turbulent conditions as Fig. 3B). Integration of Equ. (8) shows that 90% of the kinetic energy is contained between $^3/_2\, \kappa_i$ and $^2/_3\, \kappa_i$ (bold part of the δ-axis in Fig. 4). The largest eddies contain therefore most of the kinetic energy and will dominate the particle transport.

When using the spectrum prototype (Equ.(8)), we assume negligible momentum exchange between gas and particles, and no particle-particle interactions. However, the spectrum of turbulence is likely to be modified by the particles. It has been shown that large particles with high Re_p create a wake that increases the amount of turbulence, whereas small particle dampen turbulence [e.g., 43], and Elghobashi [44] proposed that this turbulence modulation is a function of S_T. Since the modulation is generated over the length scale of the particle, ε will depart from the Kolmogorov decay. Unfortunately, no generalized prototype for inhomogeneous, particle-laden flow is yet available, but a coupled Lagrangian-Eulerian approach would allow modulating the spectrum in function of the particle load.

2.3 The density profile

Consider again a fully turbulent parallel shear flow of gas with a random load of pyroclasts. Given both *(1)* the self-organization process controlled by S_T (unsteady effect of the turbulence) and *(2)* the gravity-driven stratification of concentration predicted by Σ_T (steady forcing of the gravity), the emergence of density stratification within the

pyroclastic density current is expected. Whereas large particles with a *Fall* behavior are expected to concentrate at the base of the current rapidly, small particles with a *Homogenous Transport* behavior are homogenized within the current and produce a constant density profile. The general *average* density profile of the flow is a summation of each particle size characteristic profile determined by their dynamic behavior.

Density gradients within horizontally stratified flows hinder vertical energy transfer and limit the maximum internal waves frequency to the Brunt-Väisälä frequency N. In our case, the stratification is mainly caused by particles with large Σ_T. Among these particles, those with small S_T are the most effective in hindering the energy transfer. Hence, the density profile can be used to connect a concentration gradient within the flow to a maximum eddy size δ_i and speed ΔU_i (Fig. 5):

$$N = \frac{1}{2\pi} \sqrt{-\frac{g}{\rho_0} \frac{d\rho}{dz}} = \frac{\pi \, \Delta U_i}{\delta_i} \qquad (9)$$

From the self-organization process (S_T) and the gravity-driven particle migration (Σ_T), the concentration of (coarse and/or dense) particles is higher at the base of the flow and the concentration gradient tends to be steepest at the base. Equation (9) predicts that eddies tend to be faster and smaller in strong concentration gradients (arrows in Fig. 5). Eddies formed at the base of such a turbulent dilute flow have therefore an enhanced carrying capacity compared to eddies higher above the base. The stratification process allows the flow to accommodate its loading and increases its transport capacity.

Equation (9) gives the largest possible scale of eddies in the kinetic energy spectrum for density-stratified flows. In consequence, we expect the spectrum of turbulence given

by Equ. (8) for a non-stratified flow to be modified by the density gradient (Fig. 5). The amount of shear within a stratified flow modifies also the turbulence spectrum. Qualitatively, the increase of shear raises κ_i and diminishes the turbulent decay rate towards the higher wave numbers [45]. In other words, more energy is dissipated by the larger wave number and smaller eddies take more importance in the flow dynamics, modifying the spectrum shape (arrows in Fig. 3B).

2.4 Interaction with topography

Salient parameters to describe the encounter of a density-stratified flow with an obstacle are the flow Froude number F_{Rflow} of the fastest mode of the undisturbed flow (upstream) and the dimensionless obstacle height H_d [46]:

$$F_{Rflow} = \frac{U_{fl}}{4NH} \qquad \text{and} \qquad H_d = \frac{h_{obs}}{H} \qquad (10)$$

Where U_{fl} is the mean flow speed, H the upstream flow height, and h_{obs} the obstacle height. F_{Rflow} indicates the flow hydraulic regime, sub- or supercritical. The F_{Rflow}-H_d space defines three main flow behaviors: crossing, blocking, and hydraulic jump. In the first case, the flow strata maintain their integrity during the crossing. In the second case, blocking of the lower parts of the flow occurs. In the third case, a regime change occurs and a hydraulic jump separates the two regimes.

2.5 The Dense-Dilute condition

The frequency of particle interactions is a key factor in the flow dynamics. The Dense-Dilute condition (D_D) is a measure of the importance of particle interactions within the flow [35]:

$$D_D = \frac{t_c f}{t_v} = \frac{3 \mu f}{\rho V_{rms} d}$$ (11)

Where ρ is the flow bulk density, V_{rms} the root mean square of the particle speed, f is the Reynolds number based on this velocity (Equ. (A3)), and t_c the characteristic time between particle collision given by:

$$t_c = \frac{1}{n \pi V_{rms} d^2}$$ (12)

Where n is the number density of particles. The right-hand side of Equ. (11) is obtained using that $n \pi d^3 \rho_p = \alpha \rho_p \approx \rho$, with α being the volume fraction of particles. If $D_D < 1$ (dense flow), particles do not have time to respond to the gas dynamic forces before the next collision, and the dynamics of the flow is dominated by particle-particle interactions. $D_D > 1$ (dilute flow) implies non-zero inter-particle distance.

Given the density stratification and the physical limit between a dense and a dilute flow as defined by D_D, a concentration threshold may be reached in the basal part, where granular motion will dominate. It is therefore likely that the current segregates into a basal concentrated, granular flow and an overriding dilute, turbulent, and density-stratified cloud (Fig. 6). Short-living collisional interactions dominate the resistance stresses for the rapid granular flow regime [15], and high particle concentration

suppresses turbulence-generated segregation. We therefore expect the granular flow to be composed of particles with a small D_D, either because they are not sustained by turbulence (*Fall* region), or because they are likely to gather (*Unroll* and *Margin* regions). The gathering being controlled by the transient nature of turbulence, the latter case is expected to play a minor role in the average location of the boundary. Since particles from the *Homogenous Transport* produce a constant average vertical density profile, they will be trapped in the granular flow as well, producing a poorly sorted flow. Although based on a given particle size, D_D quantifies the boundary between dense and dilute parts of the flow, because the particle size that features the lowest D_D is likely to control this boundary. Further links between collisional interaction and D_D may validate the idea that the density gradient might be so important at the boundary that a discontinuity would be formed.

3. Discussion

3.1 General implications

Our model predicts the maximum particle size that a turbulent flow can carry. For example, a pumice of 3.2 cm needs 10-m wide eddies to be faster than 30 m/s to travel within a dilute surge (*Unroll* zone, Fig. 1) and cannot be transported homogenously by a turbulent flow of gas traveling at subsonic velocities (Fig. 2). Products of large ash-flows can be examined using these critical sizes to assess their possible mode of transport.

We expect the segregation process caused by the interplay of S_T and Σ_T to occur whether the density current is initially inflated, as it probably is the case during a column collapse, or deflated, like in a dome collapse. In the latter case, the current is entirely

granular with $D_D \ll 1$ during its initiation and may inflate by incorporating air or exsolved gases. If the mixture of particle and gas becomes such that $D_D > 1$, segregation processes will take place, without the need of an upward flux of gas (e.g., [25]).

Particles in the *Unroll* zone (e.g., pumices between 0 and -4 ϕ in Fig. 4A and lithics between 1 and -3 ϕ in Fig. 4B) are likely to travel by intermittence, whenever an eddy of the appropriate size and spin occurs in the current. The kinetic energy spectrum will evolve in time as the density current travels across the landscape, modifying particle sizes affected by the *Unroll* zone. Given the asymmetric transport of this zone and that particle collection is favored at S_T near unity, the sedimentation/deposition of these particle is likely to occur in an intermittent fashion. If the current is dilute throughout its entire thickness (surge end-member), the *Unroll* zone is expected to control particles in saltation. Since particles with low S_T and Σ_T are not sedimented, the deposits of such turbulent flows will periodically exhibit a preferential settling of particles with $S_T > 1$ and $\Sigma_T \sim 1$. The layered deposit of surges may therefore represent the rapid variations of the turbulent conditions within the current.

Despite the observation that the "fines-depleted flow" defined by Walker [2] includes elutriation gas pipes, we note that the smallest median size is about 1 ϕ, whereas median sizes up to -10 ϕ have been measured [47]. Whatever processes generate fines-depleted deposits, this smallest value is consistent with the critical size for tephra homogenization by turbulent flow (Fig. 2). In other words, particles below the critical size can very easily be reentrained by a turbulent cloud and therefore are less likely to sediment.

Pyroclastic density currents have particles of different densities, ranging commonly

from 1000 kg/m^3 (pumice) to 2500 kg/m^3 (lithic). The turbulent flow illustrated in Figure

4 is able to transport pumice up to ~ -4 ϕ and homogenize (turbulent mixing) pumice

smaller than 0 ϕ (Fig. 4A, arrows I and II). Lithics smaller than -3 ϕ are carried whereas

lithic smaller than 1 ϕ are homogenized (Fig. 4B, arrows I and II). We note that a simple

"hydraulic equivalence" ($\rho_p \cdot d$) is a good first-order approximation. Widely used to

characterize particle suspension in turbulent flow, the Rouse number is a concept close

from Σ_T, although based on an average Eulerian velocity of the flow (horizontal in our

case). If this velocity is on the order of U_{rms} at κ_i, it would predict that the boundary

between transport and deposition is located at $\Sigma_T \sim 1$. Since this condition is satisfied in

the middle of the *Unroll* zone (Fig. 4), the Rouse number based on such a velocity is also

a satisfying first-order approximation of the *time-averaged* behavior of the flow.

However, the S_T–Σ_T framework is necessary to understand *transient* phenomenon such as

particle clustering, which are likely to control particle sorting, sedimentation, and the

dense-dilute threshold.

The density profile of a given particle size derived by Valentine [20] is a sole function

of the vertical velocity gradient. The Lagrangian approach reveals that the density profile

is a complex function of U_{rms}, the dusty gas bulk density (as defined by the concentration

of particles lying in the *Homogenous* zone), the turbulent spectrum shape, and the

velocity gradients. Beyond the average density profiles proposed previously (e.g.,

[20,21]), our approach highlights the potential for transient high concentration of particles

(*Margin* zone, $S_T \sim 1$), as large eddies are generated and dissipated continuously.

We would like to emphasize that S_T and Σ_T are important scaling parameters for experimental work. In other words, particle sedimentation cannot be well represented if these dimensionless numbers are not properly scaled. Although the comparison between sedimentary structures occurring under water and surge bedforms is tempting, it should be considered that, under equivalent conditions, S_T could vary of two orders of magnitude depending on the nature of the carrier phase (hot air viscosity is $\sim 1.5 \cdot 10^{-5}$ Pa·s at 300 °C whereas water is about 10^{-3} Pa·s at 20 °C). Moreover, the density contrast with the particles is greatly reduced with water as a carrier phase. Equation (1) is no longer valid because terms of the BBO equation neglected in the Raju and Meiburg [34] truncation cease to be negligible, and the full equation (A1) has to be used (see *Appendix*).

3.2 Hydraulic jump and blocking

Salient parameters to describe the interaction of a density-stratified flow with a relief are F_{Rflow} and H_d (Equ. (10)). A hydraulic jump generated by an obstacle or a break in slope causes a dramatic increase in the current depth and reduces its velocity. In the case of surges ($D_D > 1$), the potential effect of a hydraulic jump on the current can be represented by a sudden decrease of the flow speed and an increase of flow depth. The increase of depth ($\sim \delta_i$) narrows the saltation size range (*Unroll* zone in Fig. 7), and the speed reduction ($\sim U_{rms}$) lowers the maximum size the flow can transport (limit *Fall-Unroll* in Fig. 7). In this example, both the maximum size of particles carried and the critical size for homogenization are approximately reduced by a factor 2 (arrows I and II in Fig. 7). This should be expressed by an enhanced sedimentation after the jump to readjust the particle load to the new flow conditions. Experiments involving the interaction of a density current in a water tank with a ridge confirm this increase in

sedimentation (e.g., [33,48]). We predict from Fig. 7 that the load drop occurring at the jump between the two hydraulic regimes generates a moderately well sorted deposit coarser than the local average. Field studies describe ignimbrite lag breccia as very coarse material with a typical median size -3ϕ and coarser, generally lithic-rich, and often devoid of fines (e.g. [2]). Although the generation of lithic-breccia by hydraulic jumps has been evoked by several authors [22,49], they do not consider the complexity introduced by the density stratification of the flow (i.e., Equ. (10)).

Flow segregation between a dilute cloud and a granular basal part is usually not recorded in deposits because of sedimentation processes occurring at the base of the current. However, when a pyroclastic current hits a barrier or sudden relief change, the lower part of the current may be blocked, whereas the upper part rides the obstacle. The dividing streamline proposed by Valentine [20] as a blocking criterion is based on experiments only valid at low Froude number [50]. Following Baines [46], we extend the concept of blocking to high Froude number and propose that it is controlled by the density gradient-dependent F_{Rflow} and the ratio of flow to obstacle height H_d. Although blocking can occur at any level of the stratified flow, the strongest density gradient occurs at the dense-dilute boundary. The granular part of the flow is therefore the most likely to be blocked. On the high side of the obstacle, a "segregated deposit" may result, consisting of layers from specific levels within the stratified flow. Fig. 6 illustrates the blocking of the granular part of a density current that produces stratified deposits on the topographic high.

4. Conclusions

We propose a segregation mechanism of pyroclastic density currents into basal concentrated, granular flows and a overriding dilute, turbulent, and density-stratified cloud based on the Stokes number (S_T), the Stability factor (Σ_T) and the Dense-Dilute condition (D_D). Our model reveals the importance of the combined unsteady effects of turbulence and steady effects of gravity. This model is able to explain the discontinuous features between pyroclastic flows and surges while conserving the concept of a continuous spectrum. From limited assumptions, the two end-members of pyroclastic density current can be derived by using *only* intrinsic characteristics of the flow considered.

Ackowledgements

Appendix

The Bassinet-Boussinesq-Oseen (BBO) equation expresses the acceleration of the spherical particle in a nonuniform flow as [35,37]:

$$\left(1+\frac{\rho_g}{2\rho_p}\right)\frac{dv}{dt} = \frac{f}{t_v}[u(t)-v(t)] + g\left(1-\frac{\rho_g}{\rho_p}\right) + \frac{3\rho_g}{2\rho_p}\dot{u} + \sqrt{\frac{9\rho_g}{2\pi\rho_p t_v}}\left[\int_0^t \frac{\dot{u}-\dot{v}}{\sqrt{t-t'}}dt' + \frac{(u-v)_0}{\sqrt{t}}\right] \quad (A1)$$

Where t_v is the particle velocity response time given by:

$$t_v = \frac{\Delta\rho\, d^2}{18\mu} \quad (A2)$$

and f is a drag factor valid over the entire subcritical range of particle Reynolds number ($Re_p \leq 10^5$) [51]:

$$f = 1 + 0.15 Re_p^{0.687} + \frac{0.0175}{1+42500 Re_p^{-1.16}} \quad (A3)$$

With :

$$Re_p = \frac{U_T d}{\upsilon} \quad (A4)$$

Where υ is the kinematic viscosity of the gas. Particles with a small Re_p (<10) have a drag caused by the gas viscous friction along the particle body, and $f \sim 1$. For high Re_p, the drag generated by vortices in the particle wake overcomes the viscous drag, and $f \gg 1$. The right-hand side of Equ. (A1) is the sum of the viscous, gravitational, buoyancy, virtual mass, and Basset forces acting respectively on the particle. In the case of

pyroclastic density currents, the density ratio between particle and gas exceeds 10^3. It is therefore possible to truncate Equ. (A1) and use only the two first terms, namely the viscous drag and the gravity force [34]:

$$\frac{dv}{dt} = \frac{f}{t_v}[u(t) - v(t)] + g \tag{A5}$$

Nondimensionalisation by the turbulence time scale (i.e. eddy rotation time) gives Equ. (1) [52].

References

[1]   R.A.F Cas and J.V. Wright, Volcanic successions: modern and ancient, Allen & Unwin, London, 1987.

[2]   G.P.L. Walker, Ignimbrite types and ignimbrites problems, J. Volcanol. Geotherm. Res. 17, 65-88, 1983.

[3]   R.S.J Sparks, Grain size variations in ignimbrite and implications for the transport of pyroclastic flows, Sedimentology 23, 147-188, 1976.

[4]   F. Dobran, A. Neri and G. Macedonio, Numerical simulation of collapsing volcanic columns, J. Geophys. Res. 98, 4231-4259, 1993.

[5]   M.I. Bursik and A.W. Woods, The dynamics and thermodynamics of large ash flows, Bull. Volcanol. 58, 175-193, 1996.

[6]   K.H. Wohletz and M.F. Sheridan, A model of pyroclastic surge, Geol. Soc. Amer. Spec. Paper, 177-194, 1979.

[7]   R.S.J. Sparks, L. Wilson and G. Hulme, Theoretical modeling of the generation, movement, and emplacement of pyroclastic flows by column collapse, J. Geophys. Res. 83, 1727-1739, 1978.

[8]   C.J.N. Wilson, The Taupo eruption, New Zealand II. The Taupo ignimbrite, Phil. Trans. R. Soc. Lond. A314, 229-310, 1985.

[9]   J.E. Beget and A.J. Limke, Two-dimensional kinematic and rheological modeling of the 1912 pyroclastic flow, Katmai, Alaska, Bull. Volcanol. 50, 148-160, 1988.

[10]   A.H. Levine and S.W. Kieffer, Hydraulics of the August 7, 1980, pyroclastic flow at Mount St. Helens, Washington, Geology 19, 1121-1124, 1991.

[11]   M.J. Branney and P. Kokelaar, A reappraisal of ignimbrite emplacement: progressive aggradation and changes from particulate to non-particulate flow during emplacement of high-grade ignimbrite, Bull. Volcanol. 54, 504-520, 1992.

[12]   M.J. Branney and P. Kokelaar, Giant bed from a sustained catastrophic density current flowing over topography: Acatlan ignimbrite, Mexico, Geology 25, 115-118, 1997.

[13]   S.R. Hughes and T.H. Druitt, Particle fabric in a small, type-2 ignimbrite flow unit (Laacher See, Germany) and implications for emplacement dynamics, Bull. Volc. 60, 125-136, 1998.

[14] E.S. Calder, R.S.J. Sparks and M.C. Gardeweg, Erosion, transport and segregation of pumice and lithic clasts in pyroclastic flows inferred from ignimbrite at Lascar Volcano, Chile, J. Volcanol. Geotherm. Res. 104, 201-235, 2000.

[15] S. Straub, Self-organization in the rapid flow of granular material: evidence for a major flow mechanism, Geol. Rundsch. 85, 85-91, 1996.

[16] T. Takahashi and H. Tsujimoto, A mechanical model for Merapi-type pyroclastic flow, J. Volcanol. Geotherm. Res. 98, 91-115, 2000.

[17] C.J.N. Wilson, The role of fluidization in the emplacement of pyroclastic flows, 2: experimental results and their interpretation, J. Volcanol. Geotherm. Res. 20, 55-84, 1984.

[18] A.V. Anilkumar, R.S.J. Sparks and B. Sturtevant, Geological implications and applications of high-velocity two-phase flow experiments, J. Volcanol. Geotherm. Res. 56, 145-160, 1993.

[19] R.V. Fisher, Mechanism of deposition from pyroclastic flows, Am. J. Sci. 264, 350-363, 1965.

[20] G. Valentine, Statified flow in pyroclastic surges, Bull. Volcanol. 49, 616-630, 1987.

[21] T. Druitt, Emplacement of the 18 May 1980 lateral blast deposit ENE of Mount St. Helens, Washington, Bull. Volcanol. 54, 554-572, 1992.

[22] A. Freundt and H.-U. Schmincke, Lithic-enriched segregation bodies in pyroclastic flow deposits of Laacher See volcano (East Eiffel, Germany), J. Volcanol. Geotherm. Res. 25, 193-224, 1985.

[23] E.S. Calder, P.D. Cole, W.B. Dade, T.H. Druitt, R.P. Hoblitt, H.E. Huppert, L. Ritchie, R.S.J Sparks and S.R. Young, Mobility of pyroclastic flows and surges at the Soufriere Hills Volcano, Montserrat, Geophys. Res. Lett. 26, 537-540, 1999.

[24] R.S.J Sparks, J. Barclay, E.S. Calder, R.A. Herd, J.C. Komorowski, R. Luckett, G.E. Norton, L.J. Ritchie, B.Voight and A.W. Woods, Generation of a debris avalanche and violent pyroclastic density current on 26 December (Boxing Day) 1997 at Soufriere Hills volcano, Montserrat, *in*: T.H. Druitt and B.P. Kokelaar (eds) The eruption of the Soufriere Hills volcano, Montserrat 1995 to 1999, Geol. Soc., London, Memoir. in press.

[25] T. Fujii and S. Nakada, The 15 September 1991 pyroclastic flows at Unzen Volcano (Japan): a flow model for associated ash-cloud surges, J. Volcanol. Geotherm. Res. 89, 159-172, 1999.

[26] R.V. Fisher, Flow transformations in sediment gravity flows, Geology 11, 273-274, 1983.

[27] R.P. Denlinger, A model for generation of ash clouds by pyroclastic flows, with application to the 1980 eruptions at Mount St. Helens, Washington, J. Geophys. Res. 92, 10284-10298, 1987.

[28] E.M. Baer, R.V. Fisher, M. Fuller and G. Valentine, Turbulent transport and deposition of the Ito pyroclastic flow: determinations using anisotropy of magnetic susceptibility, J. Geophys. Res. 102, 22565-22586, 1997.

[29] T.H. Druitt, Pyroclastic density currents, in: Gilbert, J.S., and Sparks, R.S.J. (eds), The physics of explosive volcanic eruptions, Geol. Soc. Spec. Publ., London, v.145, 145-182, 1998.

[30] G.A. Valentine and K.H. Wohletz, Numerical models of plinian eruption columns and pyroclastic flows, J. Geophys. Res. 94, 1867-1887, 1989.

[31] A. Neri and G. Macedonio, Numerical simulation of collapsing volcanic columns with particles of two sizes, J. Geophys. Res. 101, 8153-8174, 1996.

[32] W.B. Dade and H.E. Huppert, Emplacement of the Taupo ignimbrite by a dilute turbulent flow, Nature 381, 509-512, 1996.

[33] A.W. Woods, M.I. Bursik and A.V. Kurbatov, The interaction of ash flows with ridges, Bull. Volcanol. 60, 38-51, 1998.

[34] N. Raju and E. Meiburg, The accumulation and dispersion of heavy particles in forced two-dimensional mixing layers. Part 2: The effect of gravity, Phys. Fluids 7, 1241-1264, 1995.

[35] C. Crowe, M. Sommerfeld and Y. Tsuji, Multiphase flows with droplets and particles, CRC Press, 1997.

[36] D.Z. Zhang and W.B. VanderHeyden, The effect of mesoscale structures on the macroscopic momentum equations for two-phase flows, Int. J. Multiphase Flow, in press.

[37] M.R. Maxey and J.J. Riley, Equation of motion for a small rigid sphere in a nonuniform flow, Phys. Fluids 26, 883-889, 1983.

[38] R.C. Hogan and J.N. Cuzzi, Stokes and Reynolds number dependence of preferential particle concentration in simulated three-dimensional turbulence, Physics Fluids 13, 2938-2945, 2001.

[39] P. Nielsen, Turbulence effects on the settling of suspended particles, J. Sediment. Petrol. 63, 835-838, 1993.

[40] M. Lesieur, Turbulence in fluids, Fluid Mechanics and its Applications, Kluwer Academic Publishers, 1997.

[41] O. Metais and M. Lesieur, Spectral large-eddy simulation of isotropic and stably stratified turbulence, J. Fluid Mech. 239, 157-194, 1992.

[42] A.M. Ahmed and S. Elghobashi, Direct simulation of particle dispersion in homogeneous turbulent shear flows, Phys. Fluids 13, 3346-3364, 2001.

[43] C.T. Crowe, On models for turbulence modulation in fluid-particle flows, Int. J. Multiphase Flow 26, 719-727, 2000.

[44] S. Elghobashi, On predicting particle-laden turbulent flows, Appl. Sci. Res. 52, 309-329, 1994.

[45] F.G. Jacobitz and S. Sarkar, On the shear number effect in stratified shear flow, Theoret. Comput. Fluid Dynamics 13, 171-188, 1999.

[46] P.G. Baines, Topographic effects in stratified flows, Cambridge University Press, 1995.

[47] M.J. Roobol, A.L. Smith and J.V. Wright, Lithic breccias in pyroclastic flow deposits on St. Kitts, West Indies, Bull. Volcanol. 49, 694-707, 1987.

[48] J. Alexander and S. Morris, Observations on experimental, nonchannelized, high-concentration turbidity currents and variations in deposits around obstacles, J. Sediment. Res. A64, 899-909, 1994.

[49] J.L. Macias, J.M. Espindola, M. Bursik and M.F. Sheridan, Development of lithic-breccias in the 1982 pyroclastic flow deposits of El Chichon volcano, Mexico, J. Volcanol. Geotherm. Res. 83, 173-196, 1998.

[50] W.H. Snyder, R.S. Thompson, R.E. Eskridge, R.E. Lawson, I.P. Castro, J.T. Lee, J.C.R. Hunt and Y. Ogawa, The structure of strongly stratified flow over hills: dividing-streamline concept, J. Fluid Mech. 152, 249-288, 1985.

[51] R. Clift and W.H. Gauvin, The motion of particles in turbulent gas streams, Proc. Chemeca '70, 14-28, 1970.

[52] J.E Martin and E. Meiburg, The accumulation and dispersion of heavy particles in forced two dimensional mixing layers. I. The fundamental and subharmonic cases, Phys. Fluids 6, 116-1132, 1994

Figure captions

Figure 1: The interaction of 1000 kg/m^3 particles of various sizes (x-axis) with eddies of rotation speed ΔU (y-axis) and a diameter $\delta = 10$ m. Thin curves are Stokes numbers log(S_T) and thick curves are Stability factors log(Σ_T). See text for the significance of *Fall, Unroll, Margins, Homogenous Transport,* and *Turbulent Sedimentation* zones.

Figure 2: Evolution of the particle critical size with eddy size. The critical size is the upper limit of validity of particle homogenization by turbulence. The upper and lower values of the "transition" region are defined by $S_T = 1$ and log(Σ_T) = -0.5 within the interval 5 to 50 m/s of eddy spin velocity.

Figure 3: Dynamic behavior of -3 ϕ (8 mm) particles in two characteristic eddy spaces. Patterns code the particle behavior, thin curves are log(S_T) and thick curves are log(Σ_T). A. ΔU-δ space. B. E-κ space. The kinetic energy spectrum $E(\kappa)$ is calculated for $\kappa_i = 0.25$ m^{-1} and $U_{rms} = 35$ m/s. Arrows show the effect of density stratification on the shape of the spectrum.

Figure 4: Particles behavior in the full spectrum of eddies shown in Fig. 3 in function of eddy size (y-axis) and particle size (x-axis). Bold parts of the y-axis correspond to 90% of the total kinetic energy. Patterns code the particle behavior, thin curves are log(S_T) and thick curves are log(Σ_T). Arrows I designate the maximum size transported and arrows II the maximum size

homogenized (see text). A. Particles are pumices (1000 kg/m^3). B. Particles are lithics (2500 kg/m^3).

Figure 5: Maximum eddy size δ_i and speed ΔU_i for a given concentration gradient $d\rho/dz$ in a turbulent stratified flow. Arrows show that an increase of the concentration gradient shortens and/or accelerates the more energetic eddies.

Figure 6: Schematic cross-section of a pyroclastic density current perpendicular to the flow direction with characteristic values of the three dimensionless numbers that govern the dynamics of the dilute part (S_T, Σ_T, and D_D). The end-member "surge" is obtained if the flow consists essentially of the dilute part, whereas the end-member "pyroclastic flow" has a very thin dilute portion. The right part shows a schematic density profile for three particle sizes in the dilute part. Note the total density is stratified due to the distribution of the coarse material, whereas the finest particles are homogenized throughout the flow thickness. The left part of the figure illustrates the overbanking of the dilute part. In this scenario, the dilute part overrides the obstacle, leaving stratified deposits on the topographic high.

Figure 7: Effects of a hydraulic jump from super- to subcritical regimes on the transport capacity of a turbulent flow. Patterns code the particle behavior, thin curves are log(S_T), thick curves are log(Σ_T) and particle density is 2500 kg/m^3. Flow conditions for stippled line A: $U_{rms} = 15$ m/s, $\delta_i = 20$ m. Flow conditions for stippled line B: $U_{rms} = 7.5$ m/s, $\delta_i = 50$ m.

Tables

Table 1

Symbols and Constants

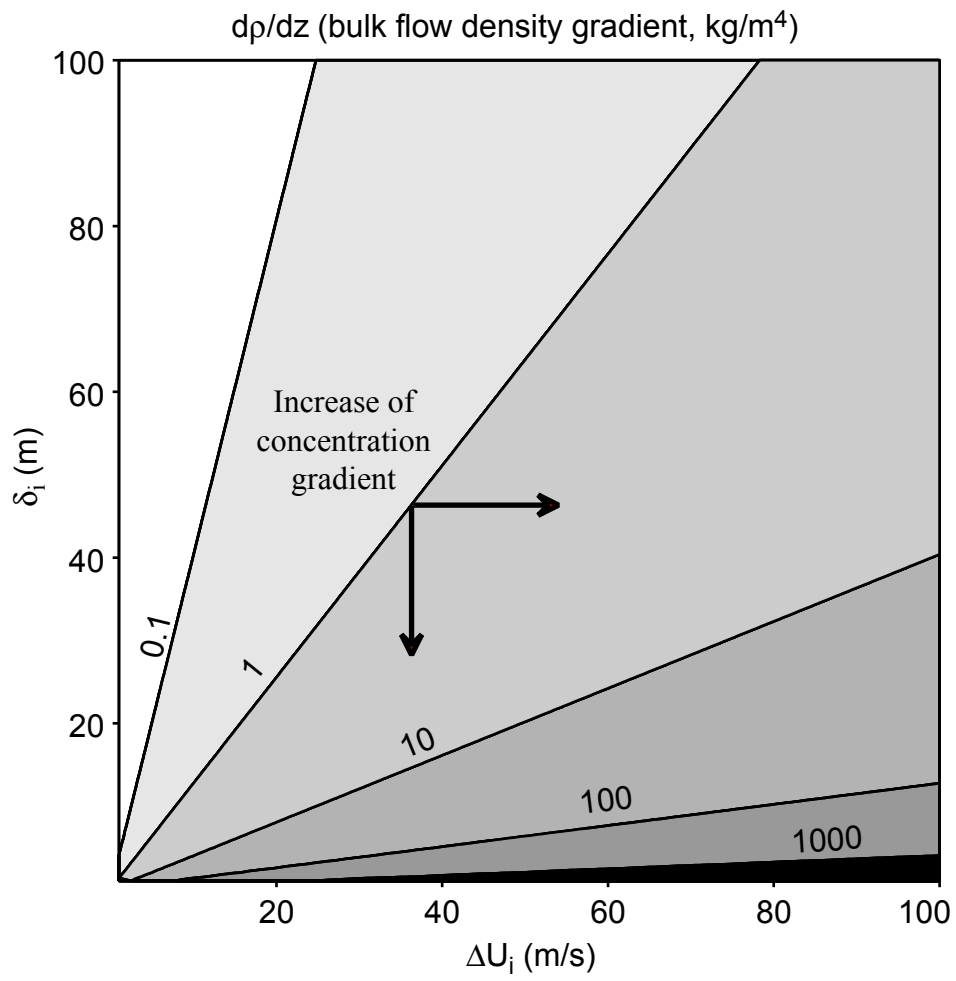|	
$u(t)$	Gas velocity (m/s)
$v(t)$	Particle velocity (m/s)
e_g	Unit vector in gravity direction
ρ	Flow bulk density (kg/m^3)
ρ_p	Particle density (kg/m^3)
ρ_g	Gas density (kg/m^3)
$\Delta\rho$	Density contrast between particles and gas (kg/m^3)
d	Particle diameter (m)
ϕ	Length unit defined as $-\log_2$ (mm)
U_T	Particle terminal fall velocity (m/s)
ΔU	Eddy revolution speed (m/s)
δ	Eddy diameter (m)
t	Time (s)
t_v	Particle response time (s)
t_c	Time between particle collisions (s)
n	Particle number density (m^{-3})
μ	Gas dynamic viscosity (1.5·10^{-5} Pa·s for air at 300 °C)
υ	Gas kinematic viscosity (3·10^{-5} m^2/s for air at 300 °C)
g	Gravity acceleration (9.81 m/s^2)
Re_p	Particle Reynolds number
f	Drag factor function of Re_p
S_T	Stokes number
F_R	Particle Froude number
Σ_T	Stability factor
D_D	Dense-Dilute condition
E	Kinetic energy per unit mass
ε	Turbulence decay rate (m^2/s^3)
κ	Eddy wave number (m^{-1})
$\kappa_i,\ \Delta U_i,\ \delta_i$	Quantities evaluated at the spectrum injection point
U_{rms}	Gas velocity root mean square (m/s)
V_{rms}	Particle velocity root mean square (m/s)
N	Brunt-Väisälä frequency (m^{-1})
U_{fl}	Mean flow speed (m/s)
F_{RFlow}	Flow Froude number
H	Upstream flow height (m)
H_d	Dimensionless obstacle height
h_{obs}	Obstacle height (m)
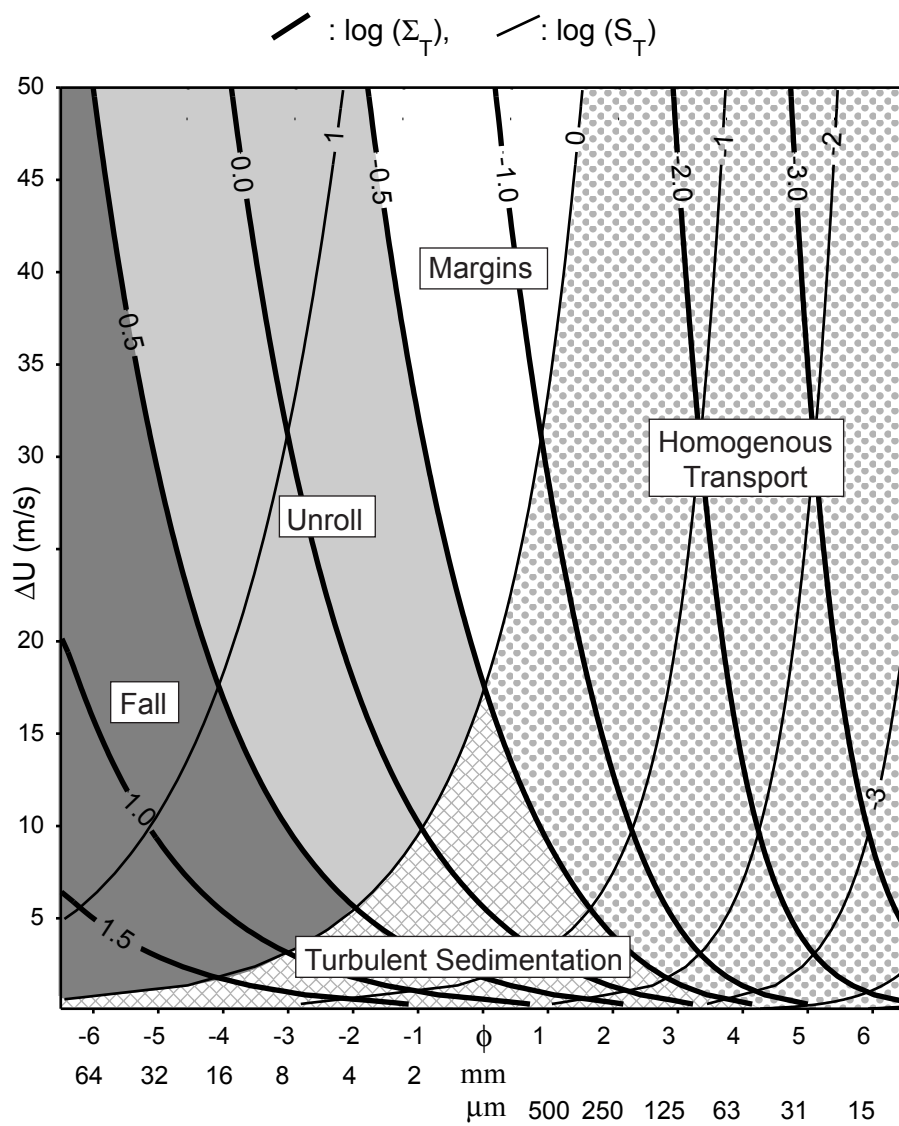
Figure 1
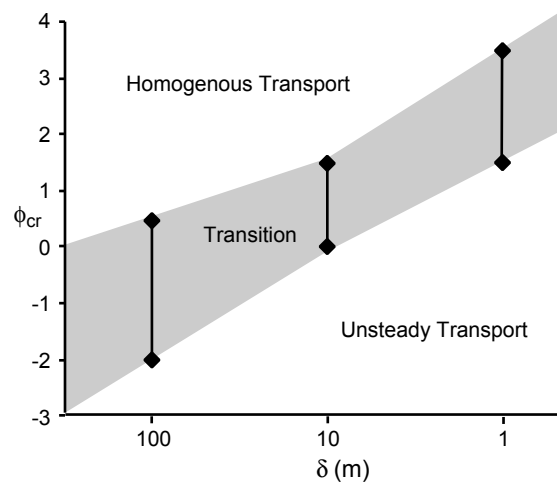
Figure 2
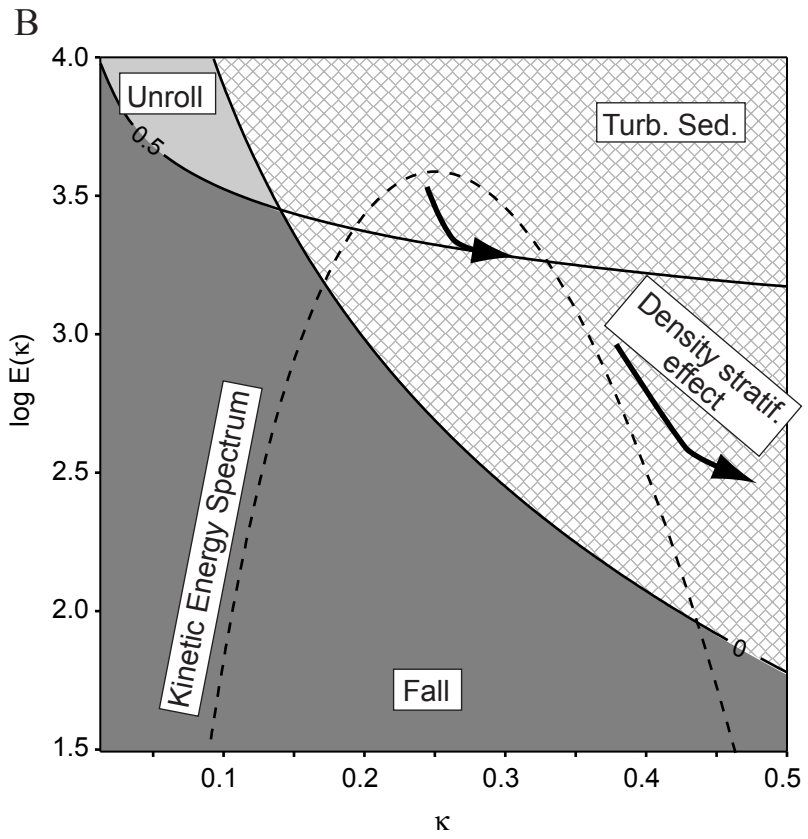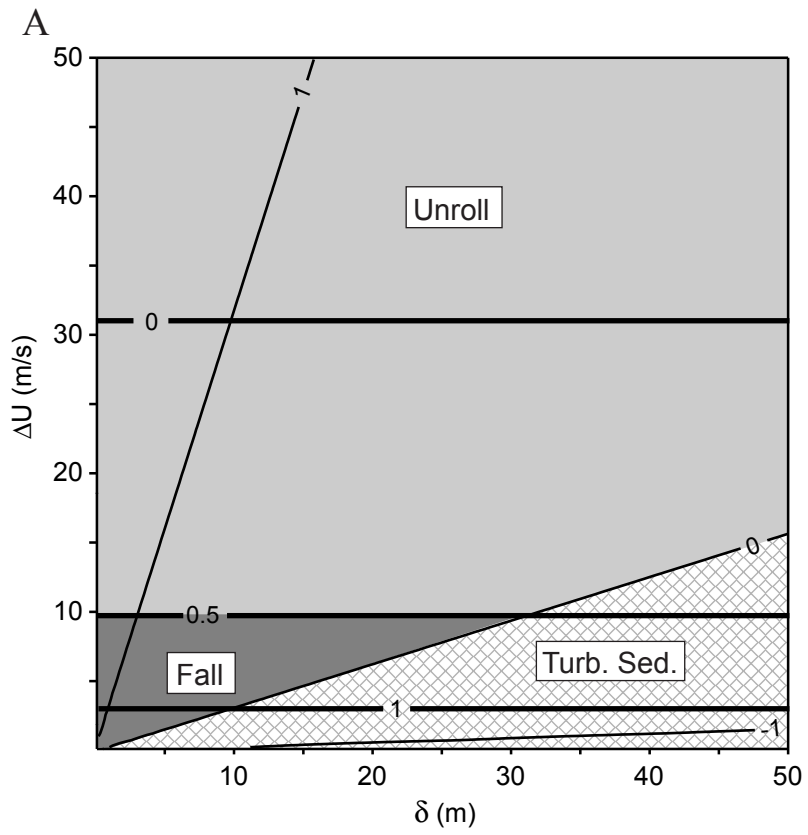
Figure 3
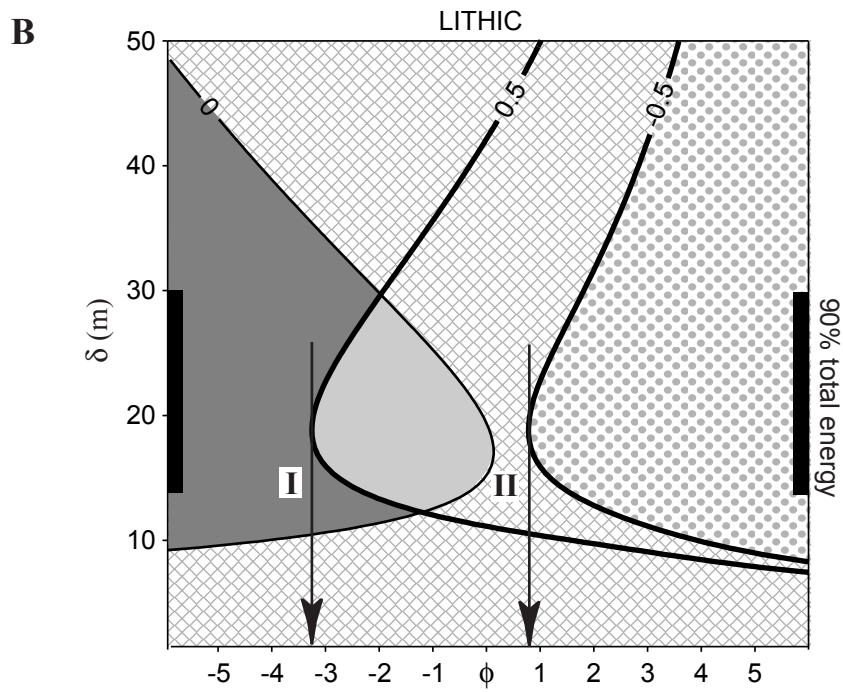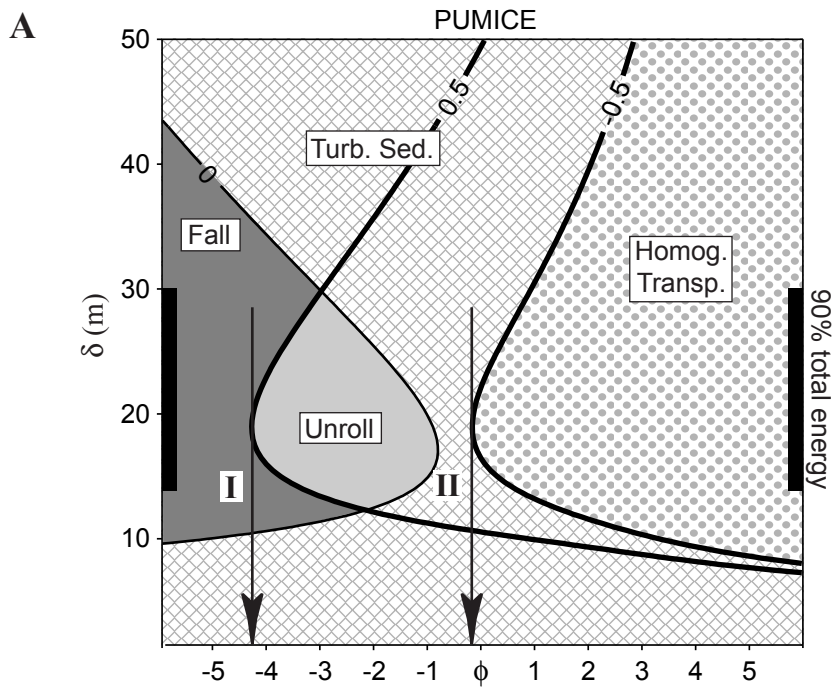
Figure 4

Figure 5

Figure 6

Figure 7